S1 Criteria for excluding grid cells from the analysis

Grid cells in which the total population fell to zero at any point during the analysis period were excluded from the analysis. This is because changes resulting in values below zero cannot be measured, which may distort the observed trends (Ushiki et al., 2019). Additionally, grid cells with a population of zero in 2000 were excluded because the covariate data discussed in Sect. 3.1.2 were unavailable for those grid cells. The treatment group comprised 2,390 grid cells, while the control group comprised 13,239 grid cells, totaling 15,629 grid cells used in the analysis.

S2 Details of data for estimating changes in the total population at the 500 m grid-cell level due to flooding

Total population data from the national census of Japan at five-year intervals from 2005 to 2020 were used (Ministry of Internal Affairs and Communications of Japan [MIC], n.d.). The data have a spatial resolution of 15″ × 22.5″ (approximately 500 m × 500 m), which is the finest resolution at which nationwide total population data are consistently available across census years. The census was conducted on 1 October in each census year.

Municipality-level data on areas affected by water-related disasters, including residential areas, were obtained from the statistical survey on flood damage conducted between 2005 and 2020 (MIC, n.d.).

Flood inundation maps of areas in Japan affected by Typhoon Hagibis (2019) and the heavy rainfall event of July 2020 were used (Geospatial Information Authority of Japan, 2019, 2020). These maps were generated using imagery and elevation data to estimate inundation depths for selected affected areas. Flood inundation maps were created for six regions affected by Typhoon Hagibis and seven regions affected by the July 2020 event. In total, flood inundation maps covering all 13 regions were used in this study. When maps were available for two different time points within the same area, they were combined. In cases where inundation depths overlapped at the two time points, the depth from the more recent map was used.

S3 Preparation of covariate data at the 500 m grid-cell level

This section describes the preparation of covariate data at the 500 m grid-cell level, as listed in Table S3. For covariates (1) through (6), we used climatological normal data for the period from 1991 to 2020 (Ministry of Land, Infrastructure, Transport and Tourism [MLIT], n.d.). Since the spatial resolution of these data is 30″ × 45″ (approximately 1 km × 1 km), the same values were assigned to all four 500 m grid cells contained within each 1 km grid cell. In regions with little or no snowfall, covariate (5) was set to zero due to the absence of data in the original dataset. Covariates (1) through (6) were treated as time-invariant variables. For covariates (7) through (20), we aimed to collect data corresponding to five years before each population count. This approach was intended to avoid post-treatment variable bias, which occurs when covariates affected by the treatment are used in the analysis, potentially leading to incorrect estimates of the treatment effect.

When data for the target year were unavailable, data from the closest available year were used instead. As a result of limited data availability, covariates (9) through (11) were treated as time-invariant variables. For covariates (7) through (11), we used point data for each facility type (MLIT, n.d.) to calculate the distance from the center of each grid cell to the nearest facility. For covariate (12), we used land price survey data provided by prefectural governments (MLIT, n.d.) and assigned to each grid cell the land price of the residential area nearest to its center. For covariate (13), we used data on densely inhabited districts (MLIT, n.d.) to create a dummy variable, assigning a value of 1 if the grid cell intersected with a densely inhabited district and 0 otherwise. For covariates (14) through (20), we used census data (MIC, n.d.) to calculate the values for each covariate. Due to aggregation adjustments for privacy protection, some grid cells had proportion values exceeding 100 % for covariates (15) through (17) and (19). Since it is unrealistic for the number of employed persons or the working-age population to exceed the total population, we capped these values at 100 %. Covariate (21) was calculated using maximum inundation depth data obtained from the fluvial flood inundation analysis conducted by Yanagihara et al. (2024), which corresponded to the 30-, 50-, 100-, and 200-year return periods for the baseline period. As the spatial resolution of these depth data is 7.5″ × 11.25″ (approximately 250 m × 250 m), values for covariate (21) were computed as the average of the four 250 m grid cells (excluding river channel cells) comprising each 500 m grid cell. Covariate (21) was treated as a time-invariant variable.

S4 Overview of the DiD method

The DiD method quantifies the impact of a treatment on an outcome variable by comparing changes in the outcome between a treatment group and a control group, before and after the treatment. A conceptual diagram of the DiD framework is presented in Fig. S1. As shown in Fig. S1, the change in the outcome variable in the treatment group that is unrelated to the treatment is estimated using the change observed in the control group, thus isolating the treatment effect. When three or more units and three or more time points are involved, the DiD method is typically implemented using the following regression equation (Baker et al., 2022):

$$O_{x,p} = \alpha_x + \beta_p + \delta T_{x,p} + e_{x,p} \quad \text{(S1)}$$

where $x = \{1, 2, \dots, m_1\}$ denotes unit indices; m_1 denotes the number of units analyzed; $p = \{1, 2, \dots, m_2\}$ denotes time-point indices; m_2 denotes the number of time points analyzed; $O_{x,p}$ denotes the outcome variable; α_x denotes unit fixed effects; β_p denotes time-point fixed effects; $T_{x,p}$ denotes the treatment variable; δ denotes the parameter for $T_{x,p}$; and $e_{x,p}$ denotes the error term. The key parameter is δ, which quantifies the treatment effect. The first term on the right-hand side controls for time-invariant unit-specific factors, while the second term also controls for time-point-specific shocks affecting all units equally. In a standard DiD model, the treatment variable $T_{x,p}$ is a binary indicator, taking the value 1 for treated units at the treatment time point and 0 otherwise. However, when evaluating the effect of treatment magnitude on the

outcome, $T_{x,p}$ can be defined as a continuous variable for treated units at the treatment time point and 0 otherwise (Kawasaki, 2021). In this study, we adopted the latter approach, defining a continuous treatment variable to represent flood magnitude.

S5 Details of the analytical method for estimating changes in the total population at the 500 m grid-cell level due to flooding

In the basic DiD model shown in Eq. (S1), the third term on the right-hand side of Eq. (1) was not included. However, if the time trends in the total population differ between the treatment and control groups, the basic DiD model fails to satisfy the parallel trends assumption. To address this issue, we followed Angrist and Pischke (2015) and added the third term to control for grid-cell-specific linear time trends and enhance the validity of the parallel trends assumption. The first term on the right-hand side of Eq. (1) controls for time-invariant confounders but not for time-varying confounders. A confounder is a variable that is correlated with the treatment indicator and influences the outcome variable. If such confounders are present, the estimated treatment effect may become biased. As with ordinary regression analysis, covariates can be incorporated into the DiD model (Morita, 2014). Therefore, a covariate vector excluding time-invariant variables is also included in Eq. (1).

In the analysis using Eq. (1), not all control-group grid cells were used. Instead, control grid cells with characteristics similar to those of the treatment grid cells were selected by using propensity score matching. This approach helps to better satisfy the parallel trends assumption by comparing treatment and control grid cells with similar characteristics (Morita, 2014). The propensity score represents the probability of receiving treatment and is estimated using multiple covariates, thereby serving as a summary measure of these covariates. The propensity scores were estimated via logistic regression analysis (Uemura et al., 2022) using covariates from 2015, the year before the flooding occurred. Since the sole purpose of the logistic regression was to estimate propensity scores, covariates were included without adjusting for multicollinearity (Uemura et al., 2022). Each treatment grid cell was matched to the control grid cell with the closest propensity score. Additionally, we did not allow the same control grid cell to be matched with multiple treatment grid cells. A one-to-one matching scheme was adopted, pairing each treatment grid cell with a single control grid cell.

S6 Indirect validation of the parallel trends assumption for estimating changes in the total population at the 500 m grid-cell level due to flooding

To examine whether statistically significant differences in the total population existed between the treatment and control grid cells before the flood event, we employed the following regression models:

$$\ln(P_{i,t}) = \gamma_i + \varepsilon_t + \zeta_i t + \boldsymbol{\eta} \boldsymbol{X}_{i,t-5}^{\text{cell}} + \sum_{\substack{s=-15 \\ s\neq -5}}^{0} \delta_s^{\text{cell}} I_{i,t-s} + e_{i,t}^{\text{cell}} \quad \text{(S2)}$$

where $I_{i,t-s}$ denotes a dummy variable equal to 1 for treated grid cells in the flood year and 0 otherwise; $s = \{-15, -10, -5, 0\}$ denotes the number of years relative to the flood event; and δ_s^{cell} denotes the parameter for $I_{i,t-s}$. To

avoid multicollinearity, the term $\delta_{-5}^{\text{cell}} I_{i,t+5}$ was excluded from the analysis. Since the flood year in this study is 2020, the parameters $\delta_{-15}^{\text{cell}}$, $\delta_{-10}^{\text{cell}}$, and δ_{0}^{cell} represent the average differences in the total population between the treatment and control grid cells in 2005, 2010, and 2020, respectively. The estimation result for Eq. (S2) is provided in Table S4. As shown in Table S4, the parameters for $I_{i,t+15}$ and $I_{i,t+10}$ are not statistically significant at the 10 % level. Therefore, we found no statistically significant differences in the total population between the treatment and control grid cells before the flood event, suggesting that the parallel trends assumption may hold.

S7 Details of data for estimating changes in the net migration rate at the municipality level due to flooding

Municipality-level data on the numbers of in-migrants and out-migrants among Japanese nationals from 2014 to 2020 were obtained from the MIC (n.d.). The numbers of in-migrants and out-migrants represent movements into and out of municipalities, respectively. Additionally, municipality-level data on the total population of Japanese residents for each year from 2014 to 2020 were obtained from the MIC (n.d.). The total population data represent the population as of 1 January of each year. Because the timing of population data aggregation differed before and after 2014, data before 2014 were excluded from the analysis. Additionally, Japanese nationals were selected as the target population because a longer time series of data was available for this group. Of the 1,902 municipalities in Japan as of 2020 (including cities, wards, towns, and villages), 1,884 were included in the analysis because complete covariate (as described in Sect. 3.2.2) and population data were available for them. Here, “wards” refer to Tokyo’s special wards and those of ordinance-designated cities. To account for municipal mergers, all data – including the numbers of in-migrants, out-migrants, and total population – were aggregated according to municipal boundaries as of 2020. This approach was consistently applied across all municipality-level datasets. The net migration rate for each municipality was calculated using the aggregated data on in-migrants, out-migrants, and total population.

Municipality-level data on the number of households affected below floor level, above floor level, and those completely destroyed from 2014 to 2020 were obtained from the statistical survey on flood damage (MIC, n.d.). These data include household damage caused not only by floods but also by sediment-related disasters and storm surges. Therefore, in this study, the number of households specifically affected by flooding was estimated by apportioning the total number of affected households based on the proportion of flood-related damage to total water-related damage to general assets. Data on general asset damage caused by water-related disasters from 2014 to 2020 were also obtained from the statistical survey on flood damage (MIC, n.d.). Damage resulting from levee breaches, overflow from leveed sections, overflow from unleveed sections, and pluvial flooding, including flooding of low-lying areas, was considered flood-related damage. Using these apportioned data and municipality-level data on the total number of households (MIC, n.d.), the proportions of households affected below floor level, above floor level, and completely destroyed by flooding were calculated for each municipality.

S8 Preparation of covariate data at the municipality level

This section describes the preparation of municipality-level covariate data, as listed in Table S6. For covariates (1) through (3), we calculated values using the number of households affected by water-related disasters (excluding flooding) and the total number of households, both obtained using a method similar to that described in Sect. S7. For covariates (4) through (9), we used climatological normal data for the 1991–2020 period (MLIT, n.d.). Because the spatial resolution of these data is 30″ × 45″ (approximately 1 km × 1 km), we calculated mean values within the habitable areas of each municipality. Habitable areas were defined by excluding forested areas and lakes from municipal boundaries using available municipal boundary data (2020), forest area data (2015), and lake data (2005) (MLIT, n.d.). In regions with little or no snowfall, covariate (8) was set to zero due to the absence of relevant data in the original dataset. Covariates (4) through (9) were treated as time-invariant variables. For covariates (10) through (29), we aimed to collect data corresponding to the year preceding each net migration rate calculation. This approach was intended to avoid post-treatment variable bias. Municipality-level data processing methods for covariates (10) through (26), (28), and (29) are summarized in Table S7. For covariate (27), we calculated the average residential land price for each municipality using land price survey data provided by prefectural governments (MLIT, n.d.).

Covariates (30) through (32) were calculated using maximum inundation depth and maximum flow velocity data obtained from the fluvial flood inundation analysis conducted by Yanagihara et al. (2024), which corresponded to the 30-, 50-, 100-, and 200-year return periods during the baseline period. Household data from 2015 (MIC, n.d.) were also used. Because the spatial resolution of the inundation depth, flow velocity, and household data is 7.5″ × 11.25″ (approximately 250 m × 250 m), values for covariates (30) through (32) were computed by aggregating the number of affected households within each municipality to calculate the expected annual number of affected households. Using the total number of households, the expected annual proportions of affected households were calculated for each municipality. The method used to calculate the number of affected households for each category was as follows. First, households located in grid cells with inundation depths of less than 45 cm were categorized as below-floor-level affected households (MLIT, 2024), excluding grid cells with maximum inundation depths below 10 cm. This exclusion was made because Yamamoto et al. (2021), whose approach was adopted in the fluvial flood damage analysis by Yanagihara et al. (2024), assumed that inundation depths of less than 10 cm would not cause flood damage. Second, households located in grid cells with inundation depths equal to or greater than 45 cm were categorized as above-floor-level affected households (MLIT, 2024), excluding grid cells identified as completely destroyed, as described below. Lastly, thresholds for collapse velocity and sliding velocity for two-story wooden buildings were calculated using the following equations, based on an example provided in the Manual for the Preparation of Flood Inundation Assumption Area Maps (4th Edition) (MLIT, 2015):

$$V_c = \sqrt{\frac{5.83}{(D_{\max} - 1.65)}} \text{ if } D_{\max} > 1.65 \quad \text{(S3)}$$

$$V_s = \begin{cases} \sqrt{\frac{35.76}{D_{\max}}} \text{ if } 0 \le D_{\max} < 2.6 \\ \sqrt{\frac{122.95 - 33.53 D_{\max}}{D_{\max}}} \text{ if } 2.6 \le D_{\max} < 3.2 \\ \sqrt{\frac{15.65}{D_{\max}}} \text{ if } D_{\max} \ge 3.2 \end{cases} \quad \text{(S4)}$$

where V_c denotes collapse velocity (m s^{-1}); V_s denotes sliding velocity (m s^{-1}); and $D_{\max}$ denotes the maximum inundation depth (m). Households located in grid cells where the maximum flow velocity exceeded either the collapse velocity threshold or the sliding velocity threshold were categorized as completely destroyed. Households located in grid cells corresponding to river channels were excluded from the calculation of affected households. Covariates (30) through (32) were treated as time-invariant variables.

S9 Method for constructing datasets for each year in the stacked regression DiD

We constructed separate datasets for each year by combining treated municipalities, control municipalities, and municipalities that had not yet experienced flooding (hereafter referred to as "not-yet-treated municipalities"). As described in Sect. S5, instead of using all control and not-yet-treated municipalities, we selected those that were similar to the treated municipalities through propensity score matching. Propensity score matching was performed using covariates other than the proportions of households affected by water-related disasters excluding flooding. Covariates from one year prior to each flood event were used, including time-invariant variables. For each year-specific dataset, data from years following the flood occurrence were excluded to account for the possibility of multiple flood events across different years. Consequently, the dataset for 2014 was cross-sectional and lacked the panel structure required for a DiD analysis. Therefore, the 2014 dataset was excluded from the analysis.

S10 Indirect validation of the parallel trends assumption for estimating changes in the net migration rate at the municipality level due to flooding

To examine whether statistically significant differences in the net migration rate existed between the treatment and control municipalities before the flood events, we employed the following regression models:

$$N_{i',t',g'} = \theta_{i',g'} + \iota_{t',g'} + \kappa_{i',g'} t' + \boldsymbol{\lambda} \boldsymbol{X}^{\text{mun}}_{i',t'-1,g'} + \sum_{\substack{\tau=-5 \\ \tau \neq -1}}^{0} \delta_{\tau}^{\text{mun}} F_{i',t'-\tau,g'} + e^{\text{mun}}_{i',t',g'} \quad \text{(S5)}$$

where $F_{i',t'-\tau,g'}$ denotes a dummy variable equal to 1 for treatment municipalities in the year of flood occurrence and 0 otherwise; $\tau = \{-5, -4, -3, -2, -1, 0\}$ denotes the number of years relative to the flood occurrence; and $\delta_{\tau}^{\text{mun}}$ denotes the parameter for $F_{i',t'-\tau,g'}$. To avoid multicollinearity, the term $\delta_{-1}^{\text{mun}} F_{i',t'+1,g'}$ was excluded from the analysis. The parameters δ_{-5}^{mun}, δ_{-4}^{mun}, δ_{-3}^{mun}, δ_{-2}^{mun}, and δ_{0}^{mun} represent the average differences in the net migration rate between the treatment and control municipalities at five years, four years, three years, and two years before the flood event, and the year of the flood

event, respectively. The estimation result for Eq. (S5) is provided in Table S8. As shown in Table S8, the parameters for $F_{i',t'+5,g'}$, $F_{i',t'+4,g'}$, $F_{i',t'+3,g'}$, and $F_{i',t'+2,g'}$ are not statistically significant at the 10 % level. Therefore, we found no statistically significant differences in the net migration rate between the treatment and control municipalities before the flood events, suggesting that the parallel trends assumption may hold.

S11 Definitions of assumed parameters for future population projections

In future population projections, survival rates, net migration rates, child–woman ratios, and sex ratios for ages 0–4 are used for each municipality. These assumed parameters are defined as follows (National Institute of Population and Social Security Research, 2018): The survival rate $SVR_{T\to T+5,S,(X \text{ to } X+4)\to(X+5 \text{ to } X+9)}$ for each municipality is defined as the proportion of individuals of sex S, aged X to $X+4$ years in year T, who survive to ages $X+5$ to $X+9$ after five years (year $T+5$). The net migration rate $NM_{T\to T+5,S,(X \text{ to } X+4)\to(X+5 \text{ to } X+9)}$ for each municipality is calculated by dividing the net number of migrants over the five-year period from year T to $T+5$, for individuals of sex S, aged X to $X+4$ years at year T, by the initial population of the same sex and age group at the beginning of the period (year T). The child–woman ratio CWR_T for each municipality is defined as the total population aged 0–4 years in year T, divided by the female population aged 15–49 years in the same year. The sex ratio for ages 0–4 SR_T for each municipality is defined as the number of males aged 0–4 per 100 females aged 0–4 in year T. These parameters are defined considering that population projections by sex and five-year age group are conducted at five-year intervals.

S12 Adjustment by uniformly scaling 250 m grid cell populations

To ensure consistency between the aggregated 250 m grid-cell population projections and the corresponding municipality-level totals by sex and five-year age group, a uniform scaling adjustment was applied as defined by the following equation:

$$aP^{250\text{m}}_{T+5,S,X\ to\ X+4} = P^{250\text{m}}_{T+5,S,X\ to\ X+4}\frac{P^{\text{mun}}_{T+5,S,X\ to\ X+4}}{P^{250\text{m,mun}}_{T+5,S,X\ to\ X+4}} \quad \text{(S6)}$$

where $aP^{250\text{m}}_{T+5,S,X\ to\ X+4}$ denotes the adjusted population (persons) by sex S and age group X to $X+4$ in year $T+5$ in each 250 m grid cell, and $P^{250\text{m,mun}}_{T+5,S,X\ to\ X+4}$ denotes the aggregated population (persons) by sex S and age group X to $X+4$ in year $T+5$ for each municipality, derived from $Pop^{250\text{m}}_{T+5,S,X\ to\ X+4}$. When Eq. (S6) was applied, including river-channel grid cells, the population could concentrate on these grid cells due to the exclusion of inundation within them. Therefore, when applying Eq. (S6), the population in river-channel grid cells was adjusted to match the population distribution obtained from the future population projections by sex and five-year age group at the 250 m grid-cell level, derived from the 1 km grid-based future population projections based on the JSSPs (NIES, 2021). The allocation method applied was the same as that used for the base-year population at the 250 m grid-cell level, as described in Table S9. As a result of adjusting the population in river-channel grid cells as described above, some municipalities had a total population within river-channel

grid cells that exceeded the corresponding municipality-level population, $Pop^{\mathrm{mun}}_{T+5,S,X\ to\ X+4}$. In such cases, Eq. (S6) was applied, including the river-channel grid cells.

S13 Methods for projecting future shortages and unused residential building land areas based on future population projections

First, we calculated the number of households at the 1 km grid-cell level using the projected population by sex and five-year age group at the 250 m grid-cell level. Specifically, following Yoshikawa et al. (2024), the number of households at the 250 m grid-cell level was projected by multiplying the population by the household head rate, and these household counts were then aggregated at the 1 km grid-cell level. The household head rate used was the value provided by Yoshikawa et al. (2024). Next, we linearly interpolated or extrapolated the relationships, obtained from Yoshikawa et al. (2024), between the number of households and both the shortage and unused residential building land areas in each 1 km grid cell, to project the corresponding shortage and unused residential building land areas for the number of households projected in this study. Linear interpolation or extrapolation was performed under the following conditions. All JSSP data from 2020 to 2100 at five-year intervals, provided by Yoshikawa et al. (2024), were used. If the projected number of households exhibited an increasing trend, linear interpolation or extrapolation was performed using data from periods of increasing household numbers. If multiple interpolation points were available, the average of the interpolated values was used as the final value. In the case of extrapolation, linear extrapolation was performed using the nearest available data point. If the projected number of households exhibited an increasing trend but no increasing trend existed in the data from Yoshikawa et al. (2024), linear interpolation or extrapolation was permitted using data from a decreasing trend. The same method was applied if the projected number of households exhibited a decreasing trend. When the projected number of households showed neither an increasing nor decreasing trend, linear interpolation or extrapolation was performed without distinguishing between decreasing and increasing processes.

S14 Spatial downscaling of future land-use data

This section describes the method used to spatially downscale future land-use data from the 1 km grid-cell level to the 250 m grid-cell level. First, the building land area at the 250 m grid-cell level in the base-year land-use data developed by Yanagihara et al. (2024) was classified into industrial, commercial/business, residential, and other building land categories. Specifically, the area ratios for each category were calculated at the 1 km grid-cell level using the base-year industrial, commercial/business, residential, and other building land areas provided by Yoshikawa et al. (2024). Assuming that the area ratios calculated at the 1 km grid-cell level were consistent across each of the 16 constituent 250 m grid cells, the building land area at the 250 m grid-cell level was proportionally allocated into each category. Next, the projected future shortages of industrial, commercial/business, and residential building land areas at the 1 km grid-cell level were spatially downscaled to the 250 m grid-cell level using the following equation:

$$A_{\mathrm{fut,shtg,250m}} = \frac{A_{\mathrm{bl,250m}}}{A_{\mathrm{bl,1km}}} A_{\mathrm{fut,shtg,1km}} \quad \text{(S7)}$$

where $A_{\mathrm{fut,shtg,250m}}$ denotes the spatially downscaled future shortage of building land area (m^2) for each category in each 250 m grid cell; $A_{\mathrm{bl,250m}}$ denotes the base-year building land area (m^2) for each category in each 250 m grid cell being downscaled; $A_{\mathrm{bl,1km}}$ denotes the base-year building land area (m^2) for each category in the 1 km grid cell containing the 250 m grid cells being downscaled; and $A_{\mathrm{fut,shtg,1km}}$ denotes the future shortage of building land area (m^2) for each category in the 1 km grid cell containing the 250 m grid cells being downscaled. The spatially downscaled future shortages of building land area for each category were then added to the corresponding base-year building land areas. Note that Eq. (S7) is not applicable when $A_{\mathrm{bl,1km}}$ equals 0 m^2. Therefore, the shortage of building land area for each category was evenly allocated among the 16 constituent 250 m grid cells within the corresponding 1 km grid cell. To keep the total land-use area constant, and following Yoshikawa et al. (2022), the combined area of paddy fields, other agricultural land, forests, wasteland, and building land in each grid cell in the base year was set as the upper limit for the increase in building land area. Additionally, any increase in building land area was offset by proportionally reducing the areas of paddy fields, other agricultural land, forests, and wasteland according to their respective area proportions. If the building land area reached the upper limit, the shortages of industrial, commercial/business, and residential building land areas were proportionally reduced while maintaining their original ratios. Finally, the future unused residential building land area at the 250 m grid-cell level was calculated using the following equation:

$$A_{\mathrm{fut,unused,250m}} = A_{\mathrm{bl,res,250m}} \frac{A_{\mathrm{fut,unused,1km}}}{A_{\mathrm{fut,unused,1km}} + A_{\mathrm{fut,res,1km}}} \quad \text{(S8)}$$

where $A_{\mathrm{fut,unused,250m}}$ denotes the spatially downscaled future unused residential building land area (m^2) in each 250 m grid cell; $A_{\mathrm{bl,res,250m}}$ denotes the residential building land area (m^2) in each 250 m grid cell in the base year; $A_{\mathrm{fut,unused,1km}}$ denotes the future unused residential building land area (m^2) in the corresponding 1 km grid cell containing the 250 m grid cells being downscaled; and $A_{\mathrm{fut,res,1km}}$ denotes the future residential building land area (m^2) in the corresponding 1 km grid cell containing the 250 m grid cells being downscaled. The future residential building land area at the 250 m grid-cell level was calculated by subtracting the unused residential building land area computed using Eq. (S8) from the base-year residential building land area. Additionally, following Yoshikawa et al. (2022), the unused residential building land area was converted into wasteland. The total building land area at the 250 m grid-cell level was obtained by summing the areas allocated to industrial, commercial/business, residential, and other building land categories, as calculated above. Following the methodology of Yanagihara et al. (2024) used for the base-year land-use data, building land areas in the future land-use dataset were classified into residential or office areas.

References

Angrist, J. D. and Pischke, J. S.: Mastering 'Metrics: The Path from Cause to Effect, Princeton University Press, Princeton, 304 pp., ISBN 9780691152844, 2015.

Baker, A. C., Larcker, D. F., and Wang, C. C. Y.: How much should we trust staggered difference-in-differences estimates? J. Financ. Econ., 144, 370–395, https://doi.org/10.1016/j.jfineco.2022.01.004, 2022.

Geospatial Information Authority of Japan: Geospatial Information Authority of Japan Technical Report: Flood inundation maps due to heavy rain caused by Typhoon Hagibis (D1-No.1011), 2019.

Geospatial Information Authority of Japan: Geospatial Information Authority of Japan Technical Report: Flood inundation maps due to the July 2020 heavy rains (D1-No.1030), 2020.

Kawasaki, K.: Econometric methods for evaluation of agricultural policy: Difference-in-differences method, Journal of Agricultural Policy Research, 35, 19–30, https://doi.org/10.34444/00000133, 2021.

Ministry of Land, Infrastructure, Transport and Tourism of Japan: Manual for the Preparation of Flood Inundation Assumption Area Maps (4th Edition), https://www.mlit.go.jp/river/bousai/main/saigai/tisiki/syozaiti/pdf/manual_kouzuishinsui_171006.pdf (last access: 7 July 2025), 2015.

Ministry of Land, Infrastructure, Transport and Tourism of Japan: Manual for Economic Evaluation of Flood Control Investment (Draft), https://www.mlit.go.jp/river/basic_info/seisaku_hyouka/gaiyou/hyouka/r604/chisui.pdf (last access: 7 July 2025), 2024.

Ministry of Land, Infrastructure, Transport and Tourism of Japan: Digital National Land Information download services, https://nlftp.mlit.go.jp/ksj/ (last access: 7 July 2025), n.d.

Ministry of Internal Affairs and Communications of Japan: Portal Site of Official Statistics of Japan (e-Stat), https://www.e-stat.go.jp/en (last access: 6 July 2025), n.d.

Morita, H.: Introduction to empirical analysis, Nippon Hyoron Sha, Tokyo, 344 pp., ISBN 978-4-535-55793-2, 2014.

National Institute for Environmental Studies, Japan: Results of Environment Research and Technology Development Fund 2-1805 (Japanese SSP Third Mesh Population Scenarios, 2nd Edition), https://adaptation-platform.nies.go.jp/data/socioeconomic/index.html (last access: 2 July 2025), 2021.

National Institute of Population and Social Security Research, Japan: Future survival rates, net migration rates, child-woman ratios, and sex ratios of the population aged 0–4 years, https://www.ipss.go.jp/pp-shicyoson/j/shicyoson18/4shihyo/chuki.pdf (last access: 7 July 2025), 2018.

Uemura, H., Matsunaka, R., and Oba, T.: Analysis on the impact of abolishing local railways on social population change by age groups in the catchment area of stations by propensity score matching, Journal of Japan Society of Civil Engineers, Ser. D3 (Infrastructure Planning and Management), 78, II_68–I_181, https://doi.org/10.2208/jscejipm.78.6_ii_168, 2022.

Yamamoto, T., Kazama, S., Touge, Y., Yanagihara, H., Tada, T., Yamashita, T., and Takizawa, H.: Evaluation of flood damage reduction throughout Japan from adaptation measures taken under a range of emissions mitigation scenarios, Clim. Change, 165, 60, https://doi.org/10.1007/s10584-021-03081-5, 2021.

Yanagihara, H., Kazama, S., Yamamoto, T., Ikemoto, A., Tada, T., and Touge, Y.: Nationwide evaluation of changes in fluvial and pluvial flood damage and the effectiveness of adaptation measures in Japan under population decline, Int. J. Disaster Risk Reduct., 110, 104605, https://doi.org/10.1016/j.ijdrr.2024.104605, 2024.

Yoshikawa, S., Takahashi, K., Wu, W., Matsuhashi, K., and Mimura, N.: Development of common socio-economic scenarios for climate change impact assessments in Japan, Geosci. Model Dev. Discuss. [preprint], https://doi.org/10.5194/gmd-2022-169, 2022.

Yoshikawa, S., Imamura, K., Yamasaki, J., Nitanai, R., Manabe, R., Murayama, A., Takahashi, K., Matsuhashi, K., and Mimura, N.: Estimation of future building area by use for data development associated with Japan SSPs, Japanese Journal of JSCE, 80, 24-27049, https://doi.org/10.2208/jscejj.24-27049, 2024.

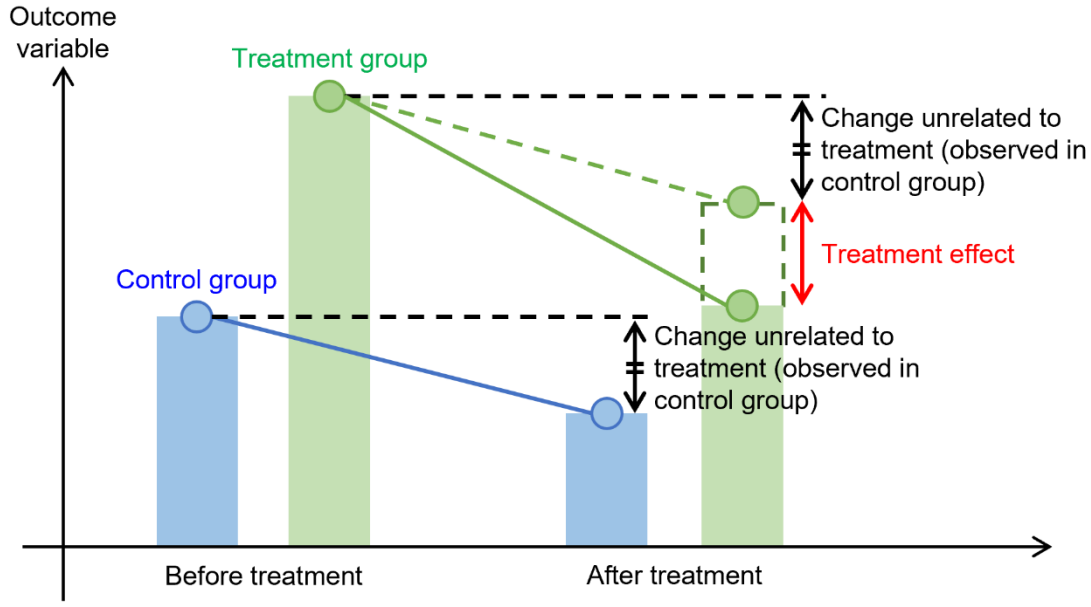

Figure S1: Conceptual diagram of the DiD framework.

Table S1: Descriptive statistics for the total population in the analyzed grid cells.

Variable	Mean	Standard deviation	Minimum	Maximum	Sample size
Total population (persons)	306	610	1	15,005	62,516

Note: Statistics are based on total population data from the 15,629 analyzed grid cells, observed at five-year intervals from 2005 to 2020.

Table S2: Descriptive statistics for the maximum inundation depth in the treatment group.

Variable	Mean	Standard deviation	Minimum	Maximum	Sample size
Maximum inundation depth (m)	2.12	1.77	0.01	14.3	2,390

Note: Statistics are based on maximum inundation depth data from the 2,390 analyzed grid cells in the treatment group.

315 **Table S3: List of covariates used in Sect. 3.1 and their descriptive statistics.**

Variable	Mean	Standard deviation	Minimum	Maximum	Sample size
(1) Climatological normal of annual precipitation (mm)	1,575.3	536.2	736.2	4,484.0	62,516
(2) Climatological normal of annual mean daily maximum temperature (°C)	17.2	3.8	7.7	27.1	62,516
(3) Climatological normal of annual mean daily minimum temperature (°C)	7.7	4.2	−2.0	21.9	62,516
(4) Climatological normal of annual mean temperature (°C)	12.2	3.8	2.8	24.3	62,516
(5) Climatological normal of annual maximum snow depth (cm)	37	45	0	304	62,516
(6) Climatological normal of annual total sunshine duration (h)	1,837.9	233.1	1,002.7	2,373.7	62,516
(7) Distance to the nearest medical facility (km)	2.2	2.7	0.0	80.5	62,516
(8) Distance to the nearest welfare facility (km)	1.6	2.0	0.0	80.0	62,516
(9) Distance to the nearest school (km)	1.9	2.1	0.0	19.3	62,516
(10) Distance to the nearest municipal office or public meeting facility (km)	1.5	1.5	0.0	20.3	62,516
(11) Distance to the nearest cultural facility (km)	2.2	2.6	0.0	66.9	62,516
(12) Land price (10,000 yen m^{-2})	3.3	4.9	0.1	121.0	62,516
(13) Dummy variable indicating densely inhabited districts	0.2	0.4	0	1	62,516
(14) Proportion of unemployed persons in the total population (%)	2.5	2.9	0	100	62,516
(15) Proportion of primary industry workers in the total population (%)	11.2	18.5	0	100	62,516
(16) Proportion of secondary industry workers in the total population (%)	12.5	9.3	0	100	62,516
(17) Proportion of tertiary industry workers in the total population (%)	24.7	13.5	0	100	62,516
(18) Total population in the surrounding eight grid cells (hundreds of persons)	21.2	40.7	0	487.4	62,516

(19) Proportion of working-age population in the total population (%)	55.4	22.6	0	100	62,516
(20) Proportion of female population in the total population (%)	51.3	7.9	0	100	62,516
(21) Expected annual inundation depth due to flooding (m)	0.01	0.02	0	0.69	62,516

Note: Statistics are based on covariate data from the 15,629 analyzed grid cells, observed at five-year intervals from 2005 to 2020. Time-invariant variables are also included.

Table S4: Estimated parameters for Eq. (S2).

	Parameter (standard error)
$I_{i,t+15}$	0.014
	(0.009)
$I_{i,t+10}$	0.002
	(0.008)
$I_{i,t}$	−0.036**
	(0.017)
Adjusted R^2	0.979
Within adjusted R^2	0.010
Sample size	19,120

Note: ***, **, and * indicate statistical significance at the 1 %, 5 %, and 10 % levels, respectively. Robust standard errors clustered at the grid-cell level are reported in parentheses. Results are shown for $I_{i,t-s}$; other results are omitted.

Table S5: Descriptive statistics for the net migration rate and the proportions of households affected by flooding in the analyzed municipalities.

Variable	Mean	Standard deviation	Minimum	Maximum	Sample size
Net migration rate (%)	−0.32	0.71	−5.38	14.28	13,188
Proportion of households affected below floor level by flooding (%)	0.05	0.39	0	18.09	13,188
Proportion of households affected above floor level by flooding (%)	0.03	0.40	0	20.77	13,188
Proportion of households that were completely destroyed by flooding (%)	0.01	0.24	0	23.01	13,188

Note: Statistics are based on data from the 1,884 analyzed municipalities over the seven-year period from 2014 to 2020.

Table S6: List of covariates used in Sect. 3.2 and their descriptive statistics.

Variable	Mean	Standard deviation	Minimum	Maximum	Sample size
(1) Proportion of households affected below floor level by water-related disasters (excluding flooding) (%)	0.01	0.11	0	4.62	13,188
(2) Proportion of households affected above floor level by water-related disasters (excluding flooding) (%)	0.00	0.17	0	17.71	13,188
(3) Proportion of households completely destroyed by water-related disasters (excluding flooding) (%)	0.00	0.05	0	5.05	13,188
(4) Climatological normal of annual precipitation (mm)	1,699.7	501.4	789.7	4,118.6	13,188
(5) Climatological normal of annual mean daily maximum temperature (°C)	18.6	3.3	9.4	27.1	13,188
(6) Climatological normal of annual mean daily minimum temperature (°C)	9.4	3.8	−1.6	21.9	13,188
(7) Climatological normal of annual mean temperature (°C)	13.7	3.4	4.5	24.2	13,188
(8) Climatological normal of annual maximum snow depth (cm)	27	43	0	309	13,188
(9) Climatological normal of annual total sunshine duration (h)	1,858.1	219.7	1,212.5	2,326.5	13,188
(10) Population per km^2 of habitable land area (persons km^{-2})	1,867	3,145	10	20,214	13,188
(11) Total area (excluding the Northern Territories and Takeshima) (ha)	19,732	23,761	347	217,767	13,188
(12) Proportion of habitable land area to total area (%)	51.6	31.0	2.4	100	13,188
(13) Taxable income per taxpayer (1,000 yen $person^{-1}$)	2,882	563	1,914	12,667	13,188
(14) Proportion of primary industry workers in the total number of workers (%)	10.0	10.1	0.0	77.0	13,188
(15) Proportion of secondary industry workers in the total number of workers (%)	24.7	8.0	1.5	52.3	13,188
(16) Proportion of tertiary industry workers in the total number of workers (%)	62.5	9.5	9.2	93.4	13,188
(17) Proportion of unemployed persons in the labor force (%)	4.2	1.4	0	17.4	13,188

(18) Number of kindergartens per 100,000 population (kindergartens)	11	16	0	335	13,188
(19) Number of elementary schools per 100,000 population (schools)	33	46	0	1,124	13,188
(20) Number of junior high schools per 100,000 population (schools)	19	42	0	1,124	13,188
(21) Number of high schools per 100,000 population (schools)	5	8	0	150	13,188
(22) Number of general hospitals per 100,000 population (hospitals)	7	7	0	72	13,188
(23) Number of elderly welfare facilities per 100,000 population (facilities)	8	14	0	275	13,188
(24) Number of childcare facilities per 100,000 population (facilities)	27	18	0	296	13,188
(25) Number of public halls per 100,000 population (halls)	41	121	0	2,834	13,188
(26) Number of libraries per 100,000 population (libraries)	5	12	0	282	13,188
(27) Land price (10,000 yen m^{-2})	5.3	10.7	0.1	290.8	13,188
(28) Proportion of working-age population in the total population (%)	56.5	5.4	33.7	73.1	13,188
(29) Proportion of female population in the total population (%)	51.4	1.4	41.3	55.9	13,188
(30) Expected annual proportion of households affected below floor level by flooding (%)	0.31	0.28	0	2.19	13,188
(31) Expected annual proportion of households affected above floor level by flooding (%)	0.21	0.31	0	2.37	13,188
(32) Expected annual proportion of households completely destroyed by flooding (%)	0.00	0.03	0	0.55	13,188

Note: Statistics are based on data from the 1,884 analyzed municipalities over the seven-year period from 2014 to 2020. Time-invariant variables are also included.

Table S7: Municipality-level data processing methods for covariates (10) through (26), (28), and (29) in Table S6.

Data	Description
Total population, working-age population, and female population [used to calculate covariates (10) and (18) through (29)]	Values from the same year as the net migration rate calculation were used because population data (total, working-age, and female population) as of 1 January were available and unaffected by flooding. However, when calculating covariates (25) and (26), total population values for Kumamoto City as a whole were used for each ward within the city.
Habitable land area [used to calculate covariates (10) and (12)]	Data for the wards of Sagamihara City and Kumamoto City were unavailable from 2013–2015. Therefore, changes in the total habitable land area of each city were apportioned to each ward based on the proportions of habitable land area data from 2016.
Number of taxpayers (income-based) and taxable income [used to calculate covariate (13)]	Since ward-level data were unavailable for ordinance-designated cities, city-level data were used for all wards within each city.
Number of primary industry workers, number of secondary industry workers, number of tertiary industry workers, total number of workers, number of unemployed persons, and labor force data [used to calculate covariates (14) through (17)]	Data for 2010, 2015, and 2020 were available. Values for intermediate years were calculated using linear interpolation. However, ward-level data for Kumamoto City in 2010 were unavailable; therefore, city-level data were used for each ward for 2010, 2015, and 2020.
Number of kindergartens, elementary schools, junior high schools, high schools, general hospitals, elderly welfare facilities, and childcare facilities [used to calculate covariates (18) through (24)]	The obtained data were used without modification.
Number of public halls and libraries [used to calculate covariates (25) and (26)]	Data were available for 2011, 2015, and 2018. Values for intermediate years were calculated by linear interpolation, except for 2019, for which the value from 2018 was used. Ward-level data for Kumamoto City in 2011 were unavailable; thus, city-level data were used for each ward for 2011, 2015, and 2018.

Note: All municipality-level data were obtained from the Portal Site of Official Statistics of Japan (e-Stat) (MIC, n.d.).

Table S8: Estimated parameters for Eq. (S5).

	Parameter (standard error)
$F_{i',t'+5,g'}$	0.039
	(0.112)
$F_{i',t'+4,g'}$	0.079
	(0.096)
$F_{i',t'+3,g'}$	0.028
	(0.074)
$F_{i',t'+2,g'}$	−0.0007
	(0.046)
$F_{i',t',g'}$	−0.117*
	(0.060)
Adjusted R^2	0.715
Within adjusted R^2	0.070
Sample size	5,512

Note: ***, **, and * indicate statistical significance at the 1 %, 5 %, and 10 % levels, respectively. Robust standard errors, clustered at the municipality level for each year-specific dataset, are reported in parentheses. Results are shown for $F_{i',t'-\tau,g'}$; other results are omitted.

Table S9: Detailed information for future population projections.

Item	Description
Target municipalities for projections	All municipalities as of 2015 were included, except those in Fukushima Prefecture, which were aggregated into one region. Populations for the special wards of Tokyo were projected separately by ward, whereas those for ordinance-designated cities were not. In total, 1,683 regions were included.
Municipality-level population in the base year	Municipality-level population data from the 2015 Population Census were used. Population figures with unknown age or sex were proportionally allocated to each sex and five-year age group according to the population composition of each municipality.
Base-year population at the 250 m grid-cell level	The 2015 population by sex and five-year age group from the 1 km grid-cell level population projections developed by NIES (based on the JSSPs; NIES, 2021) was downscaled to the 250 m grid-cell level. This downscaling was conducted using the total population at the 250 m grid-cell level in 2015. Specifically, population was allocated according to the ratio of each 250 m grid cell's total population to the total population within the corresponding 1 km grid cell.

Table S10: Estimated parameters for Eq. (1).

	Parameter (standard error)
Maximum inundation depth	−0.032*** (0.008)
Adjusted R^2	0.979
Within adjusted R^2	0.022
Sample size	19,120

Note: ***, **, and * indicate statistical significance at the 1 %, 5 %, and 10 % levels, respectively. Robust standard errors clustered at the grid-cell level are reported in parentheses. Results are shown for the maximum inundation depth; other results are omitted.

Table S11: Estimated parameters for Eq. (2).

	Parameter (standard error)
Proportion of households affected below floor level by flooding	−0.016 (0.054)
Proportion of households affected above floor level by flooding	−0.076 (0.062)
Proportion of households completely destroyed by flooding	−0.067*** (0.022)
Adjusted R^2	0.717
Within adjusted R^2	0.076
Sample size	5,512

Note: ***, **, and * indicate statistical significance at the 1 %, 5 %, and 10 % levels, respectively. Robust standard errors clustered at the municipality level for each year-specific dataset are reported in parentheses. Results are shown for the proportions of households affected by flooding; other results are omitted.